NON-EQUILIBRIUM STUDIES IN SWITCHING ARC PLASMAS IN JAPAN

Y. Tanaka[a,*], K. Tomita[b], Y. Inada[c], A. Kumada[d], K. Hidaka[d],
T. Fujino[e], K. Suzuki[f], T. Shinkai[g]

[a] *Kanazawa University, Kakuma, Kanazawa, Ishikawa 920-1192, Japan*

[b] *Kushu University, Kasuga, Fukuoka 816-8580, Japan*

[c] *Saitama University, 542 Shimo-Okubo, Sakura, Saitama 338-8570 Japan*

[d] *The University of Tokyo,7-3-1 Hongo, Bunkyo, Tokyo 113-8654, Japan*

[e] *University of Tsukuba, 1-1-1 Tennodai, Tsukuba, Ibaraki 305-8577, Japan*

[f] *Tokyo Denki University, 5 Senju Aasahi, Adachi, Tokyo 120-8551, Japan*

[g] *Tokyo University of Technology, 1404-1 Katakura, Hachioji, Tokyo 192-0982, Japan*

* tanaka@ec.t.kanazawa-u.ac.jp

Abstract. This paper briefly introduce research work examples of non-equilibrium studies in switching arcs. In understanding arc behavior, one often assumes local thermodynamic equilibrium (LTE) condition in the arc plasma. However, actual arc plasmas are not completely and not always in LTE state because of strong temperature change temporally and spatially, and high electric field application etc. Recently, we have a collaboration work in numerical simulations and experimental approaches for decaying arcs without LTE assumption. First, our numerical model is presented for decaying arcs without chemical equilibrium assumption. Secondly, two experimental methods are introduced for measuring electron density in decaying arcs without LTE assumption: Laser Thomson Scattering method and the Schack-Hartmann method. Finally, comparison results is shown between the LTE simulation, the chemically non-equilibrium simulation, and the above experimental measurements.

Keywords: Local thermodynamic equilibrium, chemically non-equilibrium, thermally non-equilibrium, electron density measurement.

1. Introduction

Thermal plasmas/arc plasmas are widely used for various applications such as plasma spray coating, rapid surface modification, fabrication of functional films, plasma arc cutting, nanopowder synthesis, and carbon nanotube synthesis etc. Switching arcs are also important applications of arc plasmas in an electric power transmission system. In understanding the behavior of thermal plasmas/arc plasmas, local thermodynamic equilibrium (LTE) models have been widely adopted. This LTE model assumes the same temperatures for kinetic energies of electrons and heavy particles. The LTE model also assumes chemically equilibrium condition, which corresponds to extremely high reaction rates for all reactions including ionization, electronic, vibrational and rotational excitations. Therefore, the LTE assumption is equivalent to one-temperature chemically equilibrium (1T-CE) model. Such the LTE model is greatly useful to predict the mass and energy transport in thermal plasmas or arcs for a conventional use, and it successfully interprets behaivor of the thermal/arc plasmas. However, more detailed understanding of the distributions of chemical species in arcs and thermal plasmas has been required for advanced thermal plasma materials processes, as well as switching arcs.

One phenomenon which causes chemically non-equilibrium effects is high spatial gradient in number density at medium-temperature or low-temperature region of arcs and thermal plasmas. In medium or low temperature regions, which are always present surrounding the high-temperature region of the arcs, the LTE assumption cannot always be established. It is necessary to account for chemically non-equilibrium effects in this case [1, 2]. Another important phenomenon for deviation from chemical equilibrium condition is a rapid change in time, i.e., a transient phenomenon in arcs and thermal plasmas. For example, switching arcs or modulated induction thermal plasmas [3, 4] are fundamentally under transient conditions. To study the transient state in arcs and thermal plasmas, attention should be paid to chemically non-equilibrium effects. On the other hand, a deviation from thermal equilibrium condition may be due to high electric field application. In switching arcs, the transient recovery voltage (TRV) is applied to a residual arc between the electrodes after current zero. Such a high voltage application may increase the electron temperature, leading to two-temperature state in residual arcs. To elucidate the aforementioned phenomena in detail, non-equilibrium effects must be considered.

This paper briefly introduces an example of non-equilibrium modeling in arc plasmas [5, 6]. In addition, some recent experiments will be introduced for decaying arcs with a detailed control of applied voltage

and injected current using some power semiconductors [7]. In the experiments, two measurement methods were adopted to determine the electron density without LTE assumption: the laser Thomson scattering method [8] and the Shack-Hartmann method [9]. Finally, we compare results between the LTE simulation, the chemically non-equilibrium simulation, and the above experimental measurements [6].

2. Non-equilibrium effects for switching arcs

For simulation of switching arcs, the LTE or one-temperature chemical equilibrium (1T-CE) models has been adopted. However, the following non-equilibrium effects may be taken into account for its further understanding:

(a) Chemically non-equilibrium effects: In arc plasmas, there are lots of reactions including molecular dissociation, association, ionization, recombination, attachment and detachment. Any reaction requires a certain finite time to reach its chemical equilibrium because the rate coefficients of reactions are also finite. On the other hand, switching arcs are essentially under transient state, and they have steep gradients in densities of chemical species. Chemically equilibrium (CE) in the switching arcs is therefore achieved only if the relaxation time for any reaction is much shorter than the characteristic time of diffusion on the particle composition as well as the transient time of the states. In other words, a rapid time change and steep gradient in switching arcs may involve chemically non-equilibrium (non-CE) state.

(b) Thermally non-equilibrium effects: In high pressure arcs, the electron temperature T_e becomes close to the heavy particle temperature T_h if the electron sufficiently transfers its kinetic energy to the heavy particle through elastic collisions compared to the energy gained from the external electric field. Establishement of thermal equilibrium state needs much less electron energy gain by the electric field than the thermal energy of electrons. Otherwise a thermal non-equilibrium condition $T_e >> T_h$ can be obtained. In switching arcs, the off-axis region has relatively lower temperature and lower electron density, which results in lower collision frequency between electrons and heavy particles. At the same time, the electric field is applied to the off-axis region as well as on-axis region in the arc. This situation may offer thermally non-equilibrium state. Furthermore, to the switching arcs, a high transient recovery voltage (TRV) is applied after current zero. This high voltage application may lead residual arcs to ones in thermally non-equilibrium state.

(c) Non-Boltzmann distribution for a population of excited particles: The population of excited particles does not follow the Boltzmann distribution if the population is more influenced by processes such as the radiative de-excitation than by thermal excitation and de-excitation. This concept is important particularly for investigating a physical state in thermal plasmas from spectroscopic observation results.

(d) Non-Maxwellian energy distribution function: The electron energy distribution function (EEDF) cannot be Maxwellian if the electron–electron energy relaxation time is much longer than the electron acceleration time by an external electric field, or if the vibrational and rotational excitation cross section is comparable with the momentum transfer cross section by the electron impact. In such cases, the Boltzmann equation should be solved considering such cross sections with an applied electric field. This situation appears in prediction of arc re-ignition phenomena in a circuit breaker.

The present paper only focuses (a) chemically non-equilibrium (non-CE) effects.

3. Numerical approaches: Modeling on chemically non-equilibrium effects

3.1. Mass conservation equation

Among various non-equilibrium effects, this section treats chemically non-equilibrium (non-CE) effects because the non-CE effects affect the behavior of arc plasmas. In non-CE state, it is difficult to adopt an LTE assumption with the mass action law such as the Guldberg–Waage and Saha equations to obtain the particle composition distribution and its transient evolution. In these cases, the following mass conservation equation for each of species j should be solved considering convection and diffusion effects and reaction rates to determine the time evolution in the particle composition distribution:

$$\frac{\partial(\rho Y_j)}{\partial t} + \nabla \cdot (\rho \boldsymbol{u} Y_j - \rho D_j \nabla Y_j) = S_j \qquad (1)$$

$$S_j = m_j \sum_{\ell=1}^{L} (\beta_{j\ell}^{r} - \beta_{j\ell}^{f}) \left(\alpha_\ell^{f} \prod_{i=1}^{N} n_i^{\beta_{i\ell}^{f}} - \alpha_\ell^{r} \prod_{i=1}^{N} n_i^{\beta_{i\ell}^{r}} \right) \qquad (2)$$

where Y_j signifies the mass fraction of species j, ρ stands for the mass density of the bulk plasma, D_j denotes the effective diffusion coefficient of j, α_ℓ^{f} and α_ℓ^{r} respectively stand for the rate coefficients of forward and backward reaction ℓ; also, n_i is the density of species i, $\beta_{i\ell}^{f}$ and $\beta_{i\ell}^{r}$ are the stoichiometric coefficient in reaction ℓ for forward and backward directions for species i, and N and L respectively denote the number of species and reactions considered. Thermodynamic and transport properties of plasmas should be calculated at each position at each time using the calculated temperature, pressure and particle composition combined with the collision integrals between the species.

3.2. Examples of chemically non-equilibrium modeling for SF$_6$ and N$_2$ arcs

Some research efforts have been undertaken to treat such chemically non-equilibrium effects in high-P and high-T plasmas for a long time [10]−[14]. Some non-equilibrium effects of SF$_6$ arc plasmas were studied theoretically or numerically from the 1990s [15]–[31]. Among these studies, chemically non-equilibrium modelling on SF$_6$ arcs had been conducted by Gleizes et al. [16]–[20] and the present authors [5],[23]–[31] .

Here, two examples of our recent non-CE modeling is introduced for SF$_6$ and N$_2$ arcs [5, 6].

3.2.1. Assumptions

The developed model assumes the following things in the decaying arc plasma for simplicity: (i) The arc plasma has the axisymmetric structure. (ii) The gas flow is laminar flow, thus the turbulent effect is neglected. (iii) The optically thin condition is assumed for radiation. (iv) All the temperatures including electron temperature, heavy particle temperature and excitation temperatures are identical. (v) Electrons, ions and neutral species have the same flow velocity. (vi) Electrode surface phenomena such as electron emission from the electrodes and surface recombination of ions were not considered for simplicity. (vii) Evaporation of the electrode and the nozzle was neglected. (viii) For SF$_6$ arcs, 19 species SF$_6$, SF$_5$, SF$_4$, SF$_3$, SF$_2$, SF, S$_2$, F$_2$, S, F, SF$^+$, S$_2^+$, F$_2^+$, SF$^-$, S$^+$, F$^+$, S$^-$, F$^-$ and e$^-$ were taken into account as constituents in SF$_6$ arc plasmas. On the other hand, N$_2$ arcs were assumed consisting of 5 species N$_2$, N$_2^+$, N, N$^+$ and e$^-$. (ix) Quasi-neutrality for electronic charge is established.

3.2.2. Governing equations

The following equations were solved to simulate an SF$_6$ decaying arc plasmas on the basis of the assumptions in the previous section as follows:

Mass:
$$\frac{D\rho}{Dt} = -\rho(\nabla \cdot \boldsymbol{u}), \tag{3}$$

Momentum:
$$\rho\frac{D\boldsymbol{u}}{Dt} = -\nabla p + \nabla \cdot \boldsymbol{\tau}, \tag{4}$$

$$\boldsymbol{\tau} = \tau_{ij} = 2\eta\left[e_{ij} - \frac{1}{3}\delta_{ij}(\nabla \cdot \boldsymbol{u})\right] \tag{5}$$

Energy:
$$\rho C_{\mathrm{v}}\frac{DT}{Dt} = -p(\nabla \cdot \boldsymbol{u}) + \nabla \cdot (\lambda_{\mathrm{tr}}\nabla T) + Q_{\mathrm{heat}} \tag{6}$$

$$Q_{\mathrm{heat}} = \sum_{j=1}^{N}\nabla \cdot (\rho D_j h_j \nabla Y_j) + \sum_{\ell}^{L}\Delta Q_\ell - P_{\mathrm{rad}} \tag{7}$$

$$h_j = \frac{1}{m_j}\left(\frac{5}{2}kT + kT^2\frac{\partial \ln Z_j}{\partial T}\right) \tag{8}$$

$$C_{\mathrm{v}} = \sum_{j=1}^{N}\frac{Y_j}{m_j}\left[\frac{3}{2}k + \frac{\partial}{\partial T}\left(kT^2\frac{\partial \ln Z_j}{\partial T}\right)\right] \tag{9}$$

Mass of species j:
$$\rho\frac{DY_j}{Dt} = \nabla \cdot (\rho D_j \nabla Y_j) + S_j, \tag{10}$$

$$S_j = m_j\sum_{\ell}^{L}(\beta_{j\ell}^{\mathrm{r}} - \beta_{j\ell}^{\mathrm{f}})\left(k_\ell^{\mathrm{f}}\prod_{i=1}^{N}n_i^{\beta_{i\ell}^{\mathrm{f}}} - k_\ell^{\mathrm{r}}\prod_{i=1}^{N}n_i^{\beta_{i\ell}^{\mathrm{r}}}\right) \tag{11}$$

The equation of state:
$$\rho = \frac{p}{\kappa \sum_j^{N}\frac{Y_j}{m_j}T} \tag{12}$$

where ρ: mass density, t: time, $\boldsymbol{u}$: gas flow vector, p: pressure, $\boldsymbol{\tau}$: stress tensor, η: viscosity, e_{ij}: unit tensor, δ_{ij}: Kronecker delta, T: temperature, C_{v}: effective specific heat at constant volume, λ_{tr}: translational thermal conductivity, D_j: effective diffusion coefficient, h_j: enthalpy of species j, Y_j: mass fraction of species j, P_{rad}: radiation power, ΔQ_ℓ: heating power from reaction heat of reaction ℓ, m_j: mass of species j, $\beta_{j\ell}$: stoichiometric coefficient of species j for reaction ℓ, $k_\ell^{\mathrm{f,r}}$: reaction rate coefficient for reaction ℓ, n_j: density of species j, κ: Boltzmann constant, $\frac{D}{Dt} = \frac{\partial}{\partial t} + \boldsymbol{u} \cdot \nabla$ is the Lagrangian derivative. Solving (10) calculates the particle composition in the arc plasma considering reaction rate, convection and diffusion effects.

For N$_2$ arc plasmas, a similar set of governing equations was solved but in forms of Fluent [6].

3.2.3. Properties and rate coefficients for reactions

The thermofluid calculation for arc plasmas needs the thermodynamic and transport properties such as mass density ρ, specific heat C_{v}, enthalpy h_j, translational thermal conductivity λ_{tr}, viscosity η, P_{rad}. These properties were calculated using the particle composition and the temperature computed and the collision integrals at each position at each calculation step. The calculation of the transport properties were carried out by the first order approximation of Chapman-Enskog method.

For SF$_6$ arcs, 64 forward reactions including the electron impact ionization, the electron attachment, the electron impact dissociation, and other chemical reactions were taken into account as well as their backward reactions [5]. These temperature-dependent coefficients were obtained in literatures [16]−[20]. In the present work, ion-ion recombination reactions such as SF$^+$ + F$^-$ + F → SF + F + F, SF$^+$ + F$^-$ + F → F$_2$ + S + F, and SF$^+$ + F$^-$ + F → F$_2$ + SF were also taken into account to study the effects of these reactions on the composition in residual arcs, especially ion remaining between the electrodes. For N$_2$ arcs, totally 22 reactions were taken into account including 11 forward reactions and their backward reactions. The rate coefficients for these reactions were obtained in literatures [6].

Figure 1 depicts the calculation space. This space was divided into 153×170 grids for the r-z two dimensional space. This configuration is the same to that in
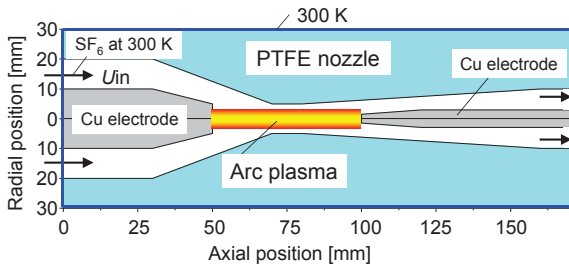
Figure 1. Calculation domain.

our experimental device. First, the 100 A dc current was applied to the arc in the steady state. Then, the transient state calculation was performed for a current stepped down from 100 A to 0 A, i.e. for free recovery condition for a fundamental study.

3.3. Examples of calculation results

3.3.1. SF$_6$ arcs: Transient distribution of F$^-$ with and without ion-ion recombination reactions

Figure 2 indicates time evolutions in F$^-$ density distribution under free recovery condition. We here treat transient behavior of F$^-$ because F$^-$ production is related to the electron density and may influence electrical conduction just around current zero [5]. In addition, we study non-CE effects on ion remaining between the electrodes. The upper panels in this figure thus show the results with consideration of ion-ion recombination reactions such as SF$^+$ + F$^-$ + F → SF + F + F, SF$^+$ + F$^-$ + F → F$_2$ + S + F, and SF$^+$ + F$^-$ + F → F$_2$ + SF, whereas the lowers are the results without consideration of ion-ion recombination reactions. By comparing the upper panel and the lower panel, we can investigate influence of ion-ion recombination reactions. At $t = 0\,\mu$s, F$^-$ has higher density about 10^{20} m^{-3} around the boundary between the arc and cold SF$_6$ gas flow. At $t = 5\,\mu$s, F$^-$ density increases rapidly with time around the fringe of the arc plasma. In particular, the arc fringe has higher F$^-$ density more than 10^{21} m^{-3} around the nozzle throat inlet, i.e. positions $55 < $ mm $z < 75$ mm. This rapid increase in F$^-$ density arises mainly from two-body dissociative attachment reactions with diatomic molecules F$_2$ + e → F$^-$ + F and SF + e → F$^-$ + S just after the current down. After that, F$^-$ density is still high around 10^{21} m^{-3} around the nozzle throat inlet until $t = 10\,\mu$s. Even at $t = 50\,\mu$s, F$^-$ becomes distributed with 10^{21} m^{-3} in whole arc region.

Consideration of the ion-ion recombination reactions influences transient behavior of F$^-$ density distribution. At $t = 5\,\mu$s, F$^-$ remains around nozzle throat inlet but in inner region. The density of F$^-$ becomes lower at the fringe of the arc plasma. This is attributed to the contribution of the ion-ion recombination reactions considered. At $t = 10$–$50\,\mu$s F$^-$ density is predicted to be lower with the ion-ion recombination. However, it is noteworthy that F$^-$ still remains with densities of 10^{20} m^{-3}. This implies
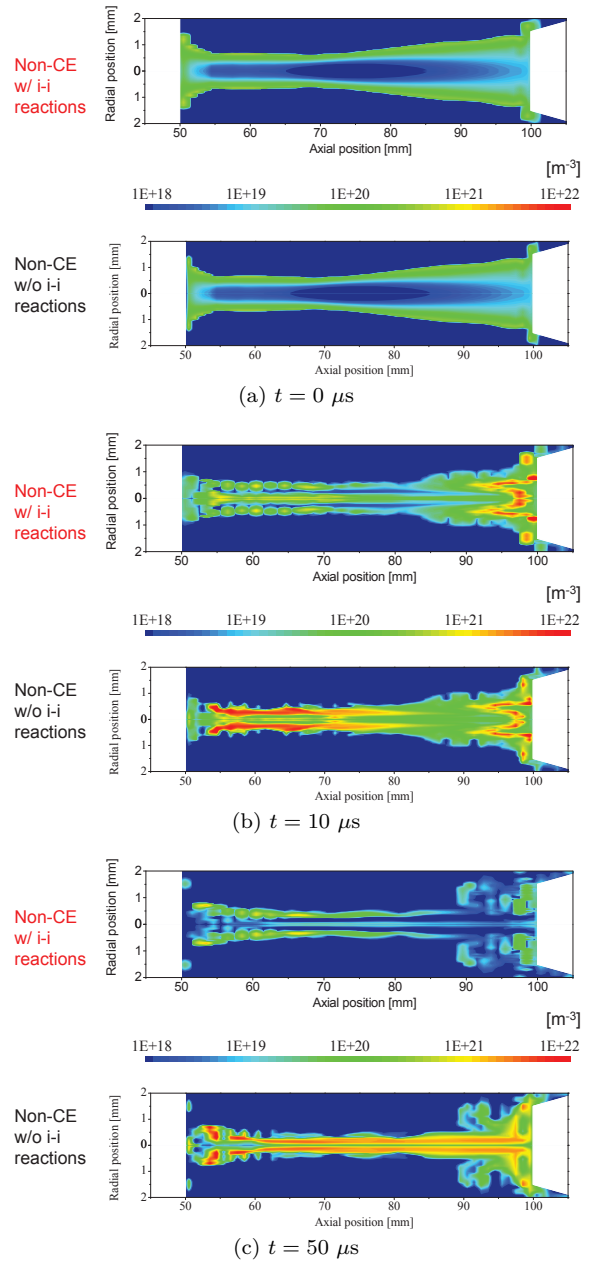

(a) $t = 0\,\mu$s

(b) $t = 10\,\mu$s

(c) $t = 50\,\mu$s

Figure 2. F$^-$ density distribution in an SF$_6$ arc at $10\,\mu$s after free recovery condition initiation. The upper panel: with ion-ion recombination; the lower panel: without ion-ion recombination.[5]

that F$^-$ is one of the key charged species for electrical conduction in an SF$_6$ residual arc.

3.3.2. N$_2$ arcs: Temperature and composition change by chemically non-equilibrium model

We calculated N$_2$ arc behavior in the same arc device using a similar non-CE model [6]. Figure 3 presents the time variations in the temperature at axial position of nozzle throat at the center axis under free recovery condition. This figure includes two results by the LTE model and the non-CE model. During $t = 0$–$15\,\mu$s, the temperature decay calculated by the non-CE model is similar to that by the LTE model.
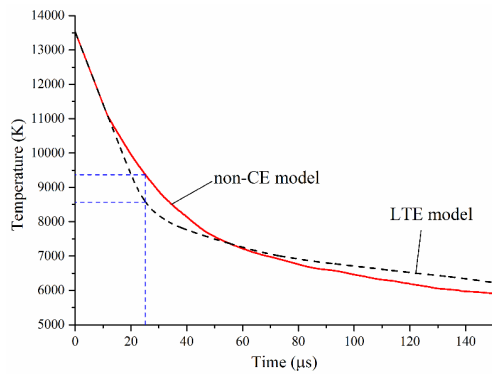
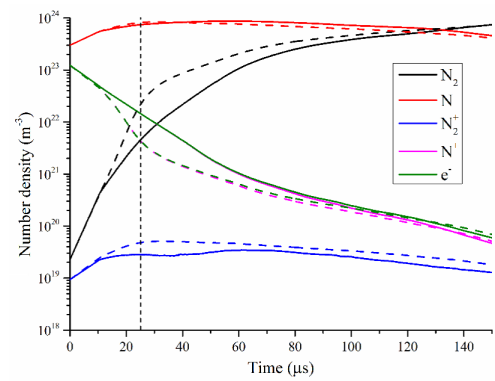*Figure 3. Time evolution in the temperature at nozzle throat in N_2 arcs [6].*

Figure 4. Time evolution of particle composition at nozzle throat in N_2 arcs [6].

The reason is that at the high temperature region more than 11000 K, the reaction rates are enough high and all the reactions tend to reach their equilibrium. At $t = 15$–$25\,\mu s$, the LTE model predicts a more rapid temperature decay than the non-CE model. After $t = 50\,\mu s$, the temperature in the non-CE model decreases with a higher decrease rate. After $t = 55\,\mu s$, the temperature in the non-CE model is lower than that by the LTE model. The above difference in the temperature decreases by the LTE model and the non-CE model is attributed to reaction rates [6].

Figure 4 shows the time evolution in particle composition at nozzle throat in N_2 arcs under free recovery condition. Solid curves are the results by the non-CE model, whereas the dashed curves are the results by the LTE model. From $t = 0$ to $10\,\mu s$, two kinds of results hardly have deviation from each other. This is because the temperature is still higher than 10000 K, and thus the reaction rates for dominant reactions are high. However, at $t = 10$–$25\,\mu s$, the electron number density, as well as the N^+ number density, decreases more slowly in the non-CE model than those in the LTE model. This higher electron density is due to the larger amount of exothermic recombination reactions. At $t > 25\,\mu s$, N_2 density predicted by the non-CE model recovers more slowly than that by the LTE model. This arises from the delay in association reaction $N + N + M \rightarrow N_2 + M$.

4. Experimental approaches: Electron density measurement without LTE assumption

We have performed the electron density measurement in an arc under free recovery condition in a arc test device without LTE assumption. This measurement result can be compared with the numerical simulation result to study arc behavior including non-equilibrium effects.

4.1. Gas-blast arc device

Figure 5 shows a photo and the cross section diagram of the nozzle used in our experiments [7]. The nozzle
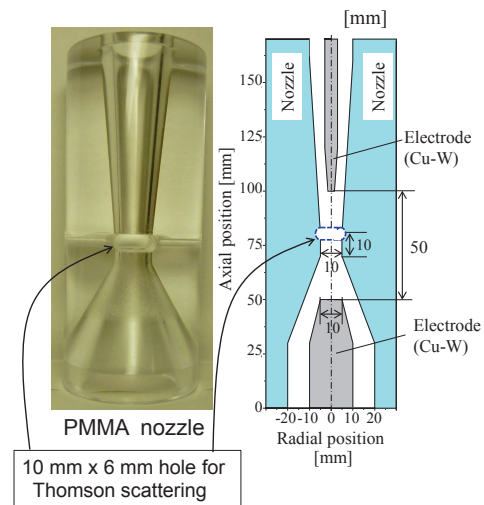

Figure 5. Configuration of the electrodes and the nozzle.

and the electrodes have a cylindrical axis-symmetric structure. The tip of the electrodes were made of copper-tungsten alloy. The lower electrode is fixed, while the upper electrode can move. The distance between the electrodes is 50 mm in open position. Between these electrodes, the arc plasma is formed. The nozzle is made of polymethyl methacrylate (PMMA), and then the visible light from the arc plasma can be observed through the nozzle. The nozzle throat width and length are 10 mm and 10 mm respectively. At the nozzle throat outlet, there is a observation hole with 10 mm × 6 mm for measuring the electron density in arc plasmas by laser Thomson scattering method. Gas flow is supplied from the downer side along the lower nozzle to the arc plasma axially.

Figure 6 depicts the experimental setup including the arc device and the electrical circuit. The nozzle and the electrodes in Fig. 5 are located inside a chamber made of stainless steel. Gas flow is supplied from a high-pressure gas tank to the lower side of the arc device. The upper electrode can open for a 50 mm stroke in about 80 ms by high-pressure air. The arc device was connected with a dc inverter current source. This
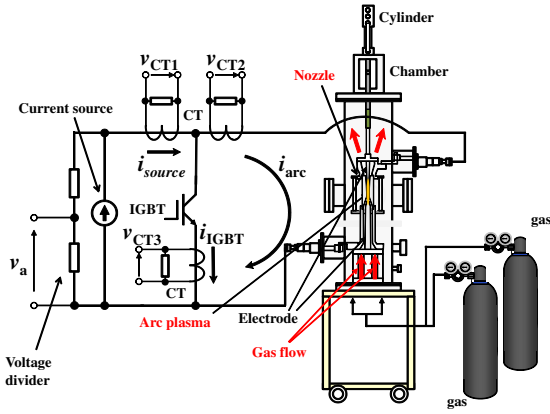
Figure 6. Experimental setup for decaying arc discharges.

Figure 7. Laser Thomson scattering spectrum measured for Ar/SF$_6$ arcs and theoretical fitting curves [8].

inverter current source is originally used for plasma cutting arcs, and it is rated at 450 V/ 300 A. In parallel to the arc device, an insulated gate bipolar transistor (IGBT) semiconductor was connected. Switching on the IGBT commutates the source current from the arc device to the IGBT element to make the arc under free recovery condition. In the experiment, we measured the source current i_source, the arc current i_arc, the IGBT current i_IGBT using the current transducers (CT). The arc voltage was measured with a CR potential divider. At different specified timing after current commutation, the electron density at the nozzle throat was measured using a laser Thomson scattering method [8].

4.1.1. Laser Thomson scattering method
Laser Thomson scattering (LTS) is well used for precise measurements of electron density in arc plasmas. When a laser light is injected to an arc plasma, free electrons in the arc plasma are excited by electromagnetic field of the laser light, resulting in the light scattering. This is called Thomson scattering. The LTS method yields local electron density and electron temperature in plasmas with high spatial and temporal resolutions without LTE assumption. In case of the arc plasma which has a short Debye length, a incident laser light with a wavelength larger than the Debye length is often used from the electron term to determine the electron density and electron temperature. We have measured the electron density in an arc under free recovery condition for our arc device depicted in Fig. 5 without LTE assumption by LTS method [8]. In this study, the second harmonic light of an Nd:YAG laser at a wavelength of 532 nm was used for LTS. The 90° scattered light from the laser path was detected.

Figure 7 indicates an example of LTS spectrum from the arc in Ar/20% SF$_6$ at a flow rate of 100 L/min [8]. We used an 2D-ICCD camera as a detector, the LTS spectra along the laser path, corresponding the radial direction of the arc, were simultaneously obtained as
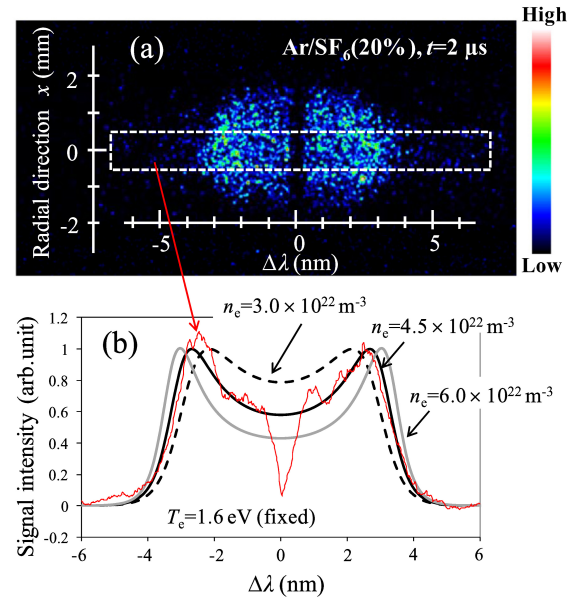
indicated in Fig. 7 (a). Figure 7 (b) shows the measured LTS spectrum at the center of the arc, and the theoretical curves of LTS for different electron densities. In this case, the electron density and the electron temperature were estimated to be 4.5×10^{22} m^{-3} and 1.6 eV, respectively, by fitting the theoretical curve to the measured spectrum.

Figure 8 presents the time evolutions in the measured electron density at the center position in nozzle throat region in Ar/SF$_6$ arcs under free recovery condition. The electric current was changed from 50 A to 0 A at $t = 0$ μs. The gas flow rate of Ar/SF$_6$ is 100 L/min. As seen, the electron density reaches to 8×10^{22} m^{-3} at 50 A at $t = 0$ μs. After current down to 0 A at $t > 0$ μs, the electron density decays almost exponentially. In particular, the 100%SF$_6$ arc has a most rapid decay in the electron density with a time constant of 10 μs. In this way, the electron density could be determined for decaying arcs at different gas mixture and different gas kinds without LTE assumption. The comparison of the results by such LTS method with the theoretically calculated result in time evolution in the electron density will be introduced in later section.

4.1.2. Shack-Hartman method
Recently, two-dimensional distribution of electron density in a plasma is measured by Shack-Hartmann type laser wavefront sensor [9]. Figure 9 shows the basic concept of a Shack-Hartmann sensor for measuring electron density distribution in an arc plasma. A Shack-Hartmann sensor is composed of an image sensor, e.g. an ICCD camera, and a sheet of micro-lens arrays. Micro-lens arrays convert the localized wavefront gradients of a laser beam into the shifts
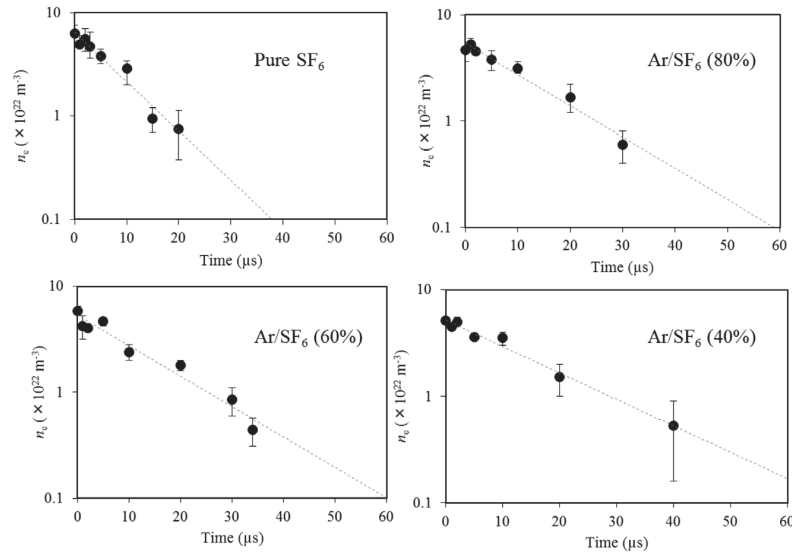
Figure 8. Temporal evolution in measured electron density in Ar/SF$_6$ (40, 60, and 80% SF$_6$) arcs current commutation under free recovery condition [8].

of the focal spot positions. A laser beam with the flat wavefront is irradiated to the arc plasmas. The laser wavefront profile through the plasma is locally distorted by different refractive indexes from the local electron density in the plasma. This distorted wavefront makes the shifted focal spot positions by the micro-lens array. This shifted spot positions were measured by the imaging sensor. This shifted displacement depends on the gradient in electron density. Thus, the electron density profile can be obtained without LTE assumption.

Figure 10 indicates the two-dimensional electron density distribution at $t = -10, 10, 30$ and $50\,\mu$s after current commutation from $50\,$A to $0\,$A to produce free recovery condition. The two-dimensional region of $4.5\,$mm $\times$ $4.5\,$mm in the nozzle throat was taken as a region for electron density measurement. The CO_2 gas is supplied from the lower region at a flow rate of $100\,$L/min. At $t = -10\,\mu$s, the dc arc with an electric current of $50\,$A is established between the electrodes. As seen in this figure, at $t = -10\,\mu$s, a two-dimensional high electron density area can be obtained with magnitudes above $10^{23}\,$m^{-3} from upstream (lower) to downstream (upper). After a current down to $0\,$A at $t > 0\,\mu$s, the electron density decreases with time under free recovery condition, and the high electron density region becomes narrower. At $t = 30\,\mu$s, the electron density decreases to $3 \times 10^{22}\,$m^{-3}. At $t = 50\,\mu$s, the upstream portion has the decreased electron density less than $10^{21}\,$m^{-3} Such a two-dimensional electron density distribution can be obtained by Shack-Hartmann method.
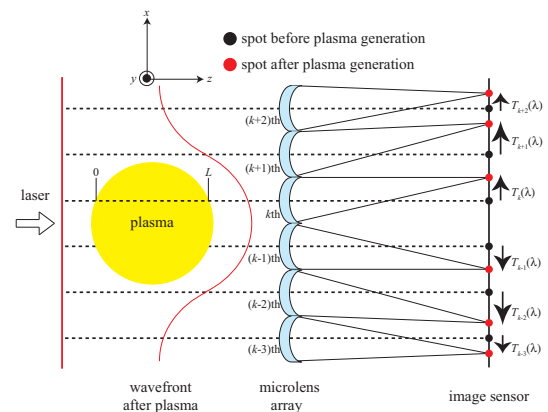

Figure 9. A schematic of a Shack-Hartmann type laser wavefront sensor for measuring electron densities in a plasma [9].

4.2. Comparison of measurement results by Laser Thomson scattering with results calculated by chemically non-equilibrium model

The electron density measured by laser Thomson scattering (LTS) method was compared with those calculated by the non-CE model and the LTE model [6]. Figure 11 shows the comparison for a N$_2$ decaying arc under free recovery condition from $50\,$A to $0\,$A. As seen in this figure, at $t = 0$–$10\,\mu$s, the measurement results fairly agree with both those by the non-CE model and the LTE model. At $t > 10\,\mu$s, the LTE model predicted a rapid decay in the electron density. However, at $t > 10\,\mu$s, the electron density measured by the LTS method is higher than that by the LTE model. On the other hand, the non-CE model predicted the electron density fairly agreeing with that
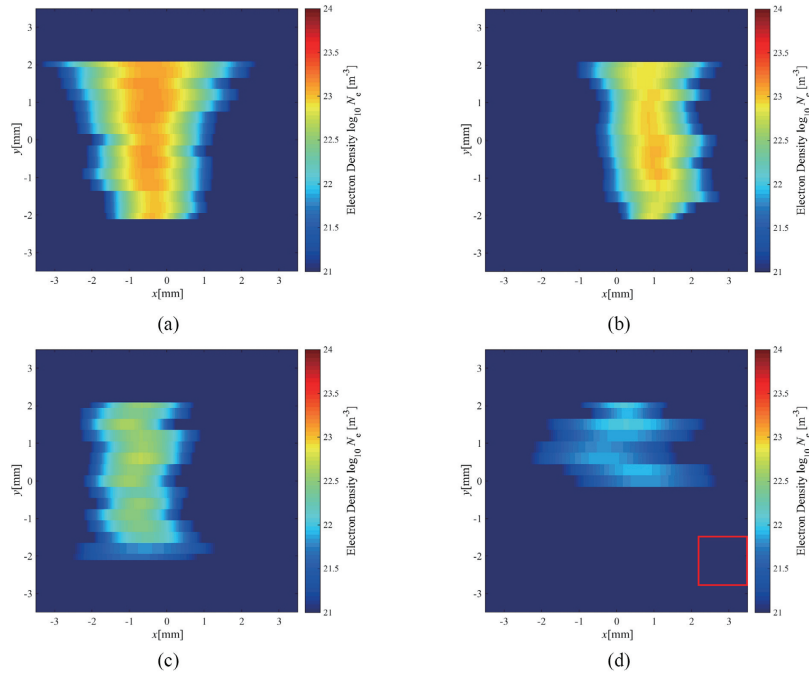
Figure 10. Two-dimensional electron density distribution in a CO_2 decaying arc plasma at t = (a) 0.1, (b) 10, (c) 30 and (d) 50 µs [9].
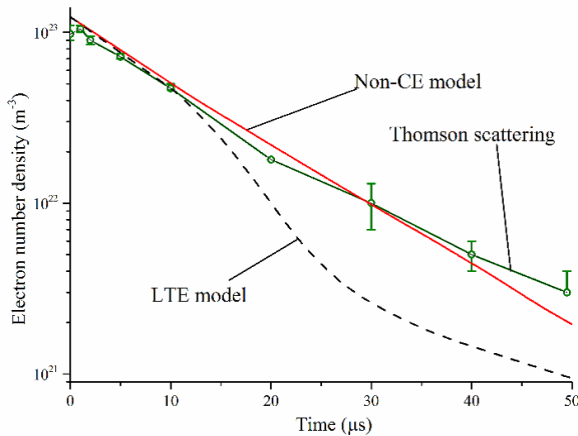

Figure 11. Comparison of electron density measurement results by laser Thomson scattering with calculation results of electron density predicted by chemically non-equilibrium model [6].

by the LTS method. The difference in electron density by the non-CE model from that by the LTE model is due to consideration of reaction rate of $N_2^+ + e \rightarrow N + N$. This implies a validity of the non-CE model, and an importance of considering non-CE effect in decaying arcs.

5. Conclusions

This paper briefly summarizes one recent approach for switching arcs in Japan: a modeling work of arc plasmas considering non-equilibrium effects in high-pressure high-temperature plasmas, and experimental works for electron density measurement without LTE assumption. Results indicates an importance of chemically non-equilibrium effects in a switching arc.

References

[1] A. Gleizes et al. Thermal plasma modelling. *J. Phys. D: Appl. Phys.*, 38(9):R153, 2005. doi:10.1088/0022-3727/38/9/R01

[2] V. Rat et al. Treatment of non-equilibrium phenomena in thermal plasma flows. *J. Phys. D: Appl. Phys.*, 41(18):183001, 2008. doi:10.1088/0022-3727/41/18/183001

[3] Y. Tanaka, T. Muroya, K. Hayashi, and Y. Uesugi. Control of nitrogen atomic density and enthalpy flow into reaction chamber in Ar-N_2 pulse-modulated induction thermal plasmas. *IEEE Trans. Plasma Sci.*, 35:197-203, 2007. doi:10.1109/TPS.2007.892709

[4] Y. Tanaka, K. Hayashi, T. Nakamura, and Y. Uesugi. Influence of ontime on increased number density of excited nitrogen atom in pulse modulated induction thermal plasmas. *J. Phys. D: Appl. Phys.*, 41(18):185203, 2008. doi:10.1088/0022-3727/41/18/185203

[5] Y. Tanaka, K. Suzuki, and T. Iijima. Role of ion-ion recombinations in decaying SF_6 arc plasmas. *Proc.21th Int. Conf. Gas Discharges and their Applications GD2016*, A15, pp.57-60, 2016.

[6] H. Sun, Y. Tanaka, K. Tomita, Y. Wu, M. Rong, Y. Uesugi, and T. Ishijima. Computational non-chemically equilibrium model on the current zero simulation in a model N_2 circuit breaker under the free recovery condition. *J. Phys. D: Appl. Phys.*, 49(5):055204, 2015. doi:10.1088/0022-3727/49/5/055204

[7] Y.Tanaka, T.Nakano, H.Shimizu, K.Tomita, and K.Suzuki. Fundamental investigation technique on gas-blast arc behaviors in decaying and re-ignition processes using power semiconductors. *Trans. IEEJ PE*, 135(11):661-668, 2015. doi:10.1541/ieejpes.135.661

[8] K. Tomita, D. Gojima, T. Shimizu, K. Uchino, T. Nakano, Y. Tanaka, K. Suzuki, T. Iijima, and T. Shinkai. Thomson scattering diagnostics of SF_6 gas-blasted arcs confined by a nozzle under free recovery conditions. *J. Phys. D: Appl. Phys.*, 48(26):265201, 2015. doi:10.1088/0022-3727/48/26/265201

[9] Y. Inada, A. Kumada, H. Ikeda, K. Hidaka, T. Nakano, K. Murai, Y. Tanaka, and T. Shinkai. Comparative study on extinction process of gas-blasted air and CO_2 arc discharge using twodimensional electron density imaging sensor. *J. Phys. D: Appl. Phys.*, 50:175202, 2017. doi:10.1088/1361-6463/aa652b

[10] G.Y. Zhao, J. Mostaghimi, and M.I. Boulos. The induction plasma chemical reactor: Part II. Kinetic Model. *Plasma Chem. Plasma Process.*, 10(1):151–166, 1990. doi:10.1007/BF01460453

[11] J. B. Belhaouari, J.J. Gonzalez, and A. Gleizes. Simulation of a decaying SF_6 arc plasma: hydrodynamic and kinetic coupling study. *J. Phys. D: Appl. Phys.*, 31(10):1219–1232, 1998. doi:10.1088/0022-3727/31/10/014

[12] A. B. Murphy and T. McAllister. Modeling of the physics and chemistry of thermal plasma waste destruction. *Phys. Plasmas*, 8(5):2565–2571, 2001. doi:10.1063/1.1345884

[13] Y. Tanaka, T. Michishita, and Y. Uesugi. Hydrodynamic chemical non-equilibrium model of a pulsed arc discharge in dry air at atmospheric pressure. *Plasma Sources Sci.& Technol.*, 14(1):134–151, 2005. doi:10.1088/0963-0252/14/1/016

[14] S.A. Al-Mamun, Y. Tanaka, and Y. Uesugi. Chemically non-equilibrium modelling of Ar inductively coupled thermal plasma with C-H-O systems. *J. Plasma & Fusion Res. Ser.*, 8:1243–1247, 2009.

[15] A. Gleizes, F. Mbolidi, and A.A.M. Habib. Kinetic model of a decaying SF_6 plasma over the temperature range 12000 K to 3000 K. *Plasma Sources Sci. Technol.*, 2(3):173-179, 1993. doi:10.1088/0963-0252/2/3/007

[16] R. Girard, J.J. Gonzalez, and A. Gleizes. Modelling of a two-temperature SF_6 arc plasma during extinction. *J. Phys. D: Appl. Phys.*, 32(11):1229-1238, 1999. doi:10.1088/0022-3727/32/11/308

[17] A. Gleizes, B. Chervy, and J.J. Gonzalez. Calculation of a two-temperature plasma composition: bases and application to SF_6. *J. Phys. D: Appl. Phys.*, 32(16):2060-2067, 1999. doi:10.1088/0022-3727/32/16/315

[18] R. Girard, J.B. Belhaouari, J.J. Gonzalez, and A. Gleizes. A two-temperature kinetic model of SF_6 plasma. *J. Phys. D: Appl. Phys.*, 32(22):2890-2901, 1999. doi:10.1088/0022-3727/32/22/311

[19] I. Coll, A.M. Casanovas, L. Vial, A. Gleizes, and J. Casanovas. Chemical kinetics modelling of a decaying SF_6 arc plasma in the presence of a solid organic insulator, copper, oxygen and water. *J. Phys. D: Appl. Phys.*, 33(3):221-229, 2000. doi:10.1088/0022-3727/33/3/308

[20] J.J. Gonzalez, R. Girard, and A. Gleizes. Decay and post-arc phases of a SF_6 arc plasma: a thermal and chemical non-equilibrium model. *J. Phys. D: Appl. Phys.*, 33(21):2759-2768, 2000. doi:10.1088/0022-3727/33/21/314

[21] Y. Tanaka, Y. Yokomizu, M. Ishikawa, and T. Matsumura. Electrical conductivity and enthalpy of two-temperature SF_6 plasma at a pressure of 0.1 MPa. *Proc. Int. Conf. on Electr. Eng. '97*, 726-729, 1997.

[22] T. Matsumura, Y. Yokomizu, T. Matsubara, and Y. Tanaka. Electrical conductivity and enthalpy of SF_6 plasma in two-temperature state. *Proc. 12th Int. Conf. on Gas Discharges & Their Appl.*, I, 94-97, 1997.

[23] Y. Tanaka, Y. Yokomizu, T. Matsubara, and T. Matsumura. Particle composition of two-temperature SF_6 plasma in pressure range from 0.1 to 1 MPa. *Proc. 12th Int. Conf. on Gas Discharges & Their Appl.*, II, 566-569, 1997.

[24] T. Matsubara, Y. Tanaka, Y. Yokomizu, and T. Matsumura. Deviation from local thermal equilibrium in SF_6 post-arc channel exposed to transient recovery voltage. *1998 IEEE Int. Conf. on Plasma Sci.*, 150, 1998. doi:10.1109/PLASMA.1998.677556

[25] Y. Tanaka, T. Matsubara, Y. Yokomizu, T. Matsumura, and T. Sakuta. Calculation of SF_6 plasma composition in two-temperature steady state using reaction kinetics. *Proc. Int. Conf. on Electr. Eng. ICEE'98*, 583-586, 1998.

[26] Y. Tanaka and T. Sakuta. Numerical approach for analysing transient behaviour of SF_6 induction thermal plasma using reaction kinetics. *Proc. Int. Symp. on Plasma Chem.*, 245-250, 1999.

[27] Y. Tanaka and K. Suzuki. *Proc. Int. Conf. Elect. Power Equip. ICEPE-ST 2011*, 2011.

[28] Y. Tanaka, K.Suzuki, T.Iijima, and T.Shinkai. Development of a thermally and chemically non-equilibrium model for decaying SF_6 arc plasmas. *2nd Int. Conf. Electric Power Equip. ICEPE-ST 2013*, 2013. doi:10.1109/ICEPE-ST.2013.6804353

[29] Y. Tanaka and K.Suzuki. Numerical Simulation on Two-Temperature Chemically Non-Equilibrium States in Decaying SF_6 Arcs after Application of Recovery Voltage. *20th Int. Conf. Gas Discharges and Their Appl. GD2014*, A34, pp.179-182, 2014.

[30] Y. Tanaka and K. Suzuki. Non-Equilibrium Effects on SF_6 Arc Plasmas in Decaying Phases. *Int. Conf. Electric Power Equipment ICEPE-ST 2015*, GO-181, 2015. doi:10.1109/ICEPE-ST.2015.7368379

[31] Y. Tanaka and K.Suzuki. A Fundamental Study on Chemically Non-Equilibrium State in Decaying SF_6 Arc Plasmas. *Int.Conf.Fluid Dynamics (ICFD2016)*, 2016.